This is a preprint, the final version is subject to change, of the American Mineralogist (MSA)
Cite as Authors (Year) Title. American Mineralogist, in press.
(DOI will not work until issue is live.) DOI: http://dx.doi.org/10.2138/am-2015-5025

Structural effects on incorporated water in carbonated apatites

REVISION 1

Jennifer E. Goldenberg[1], Zachary Wilt[1], Demetra V. Schermerhorn[1], Jill D. Pasteris[2], and Claude H. Yoder[1]*

[1]Franklin and Marshall College, Department of Chemistry, Lancaster, PA 17603

[2]Washington University in St. Louis, Department of Earth and Planetary Sciences, St. Louis, MO 63130-4899

*To whom correspondence should be addressed. Email: claude.yoder@fandm.edu

Running title: Structural effects on incorporated water in carbonated apatites

Revision submitted to American Mineralogist, July, 2014

Always consult and cite the final, published document. See http://www.minsocam.org or GeoscienceWorld

Abstract

Confirmation of structural H_2O in apatites using ^2H solid state NMR spectroscopy has been followed by the determination of the number of molecules of H_2O per unit cell (MPUC) using thermal gravimetric analysis (TGA) in 10 series of carbonated apatites (CMApX; $M_{10}(PO_4)_6X_2$ = MApX) containing the divalent cations (M) calcium, strontium, barium, and lead, and monovalent anions (X) OH^-, F^-, and Cl^-. For many of the series, the average MPUC ranges from ca. 1.5 – 2.5 and is independent of the concentration (wt%) of carbonate. For other series, the average MPUC is as low as ca. 0.8 or as high as ca. 4.0. We have found for six of the series, i.e., those in which carbonate predominantly (>90%) substitutes for phosphate, that the average MPUC correlates with cation and anion atomic radii, with unit cell axial lengths, and, especially, with our calculations of the void space available in the c-axis channels.

We speculate that the volume of the channels in apatites affects the ability of H_2O to occupy channel sites. In most low-temperature apatites of the type $M_{10}(PO_4)_6X_2$ that have been studied, carbonate prefers to substitute for phosphate (B-type substitution) rather than for monovalent anions in channel sites (A-type substitution), even though computer simulations indicate that carbonate is more thermodynamically stable in the channel sites rather than the phosphate sites. In apatites with nearly total B-type carbonate substitution, there is no relationship between the number of molecules of H_2O in the channels and the weight percent carbonate in the apatite. This lack of correlation would be expected when

there is no competition within the channel between H_2O and carbonate occupancy. In apatites with greater channel volumes, however, we infer that increased ease of carbonate incorporation in the channels also increases competition between H_2O and carbonate. The originally incorporated amount of H_2O is diminished to accommodate the thermodynamically favored carbonate ion substitution in the channels. We further speculate that these scenarios are most easily rationalized by incorporation of H_2O early in the formation of nascent crystallites of apatites formed in aqueous solution, with carbonate entering the newly formed channels later and, in some cases, with difficulty.

Key words: Water, carbonate, apatite, Rietveld, channel

Introduction

The association of water with apatites has long been recognized but the presence of incorporated molecular H_2O has only recently been verified by incorporation of D_2O in the apatite structure and identification of the D_2O by IR, Raman, and ^2H solid state NMR spectroscopy (Yoder et al. 2012c; Pasteris et al. 2014). The presence of this molecular species in the c-axis channels of apatites may be a factor in the preference of synthetic low temperature (< 100°C) apatites for B-type carbonate substitution for phosphate, in spite of the likely thermodynamic preference for substitution of the channel ion via A- or mixed AB-type carbonate substitution (Peroos and de Leeuw 2006). The charge imbalance caused by

B-type substitution of CO_3^{2-} or HPO_4^{2-} for PO_4^{3-} typically leads to anion vacancies in the channel site. Hydrogen-bonding of H_2O to phosphate oxygen atoms as well as charge-dipole interactions may help stabilize structures in which many of the channel anions have been removed. Finally, the presence of channel H_2O may account for rehydroxylation of initial carbonated, hydroxyl-deficient apatites that undergo thermal decarbonation (Pasteris et al. 2012).

We have continued our exploration of structurally incorporated H_2O by synthesizing carbonated apatites of calcium, strontium, barium, and lead containing the monovalent anions OH^-, F^-, Cl^-, and Br^-. The amount of structural H_2O in 76 synthesized carbonated apatites (CMApX) has been determined by thermogravimetric analysis (TGA), and the cell parameters of a subset of these apatites have been determined by Rietveld analysis of X-ray diffraction data. Our objective has been to identify structural parameters and lattice interactions that are responsible for the number of H_2O molecules incorporated in the unit cell.

EXPERIMENTAL METHODS

Syntheses

All syntheses utilized aqueous ion-combination reactions of metal nitrates or metal halides (when the monovalent anion was a halide) with sodium or ammonium dihydrogen

phosphate and sodium or ammonium bicarbonate. In some cases, a sodium or ammonium halide was added as the source of the monovalent anion. After digestion periods ranging from 2 h to 2 d at temperatures ranging from 60 to 90 °C, the products were filtered under vacuum, carefully washed with water, and then dried overnight in vacuum. The syntheses have been reported as follows: CCaApOH (Flora et al. 2004, Yoder et al. 2012a), CCaApF (Yoder et al 2012a), CSrApX, X = F, Cl, OH (Weidner et al. 2014); CBaApOH and CBaApCl (Yoder et al. 2012b); CPbApOH and CPbApCl (Sternlieb et al. 2010); CPbApF and CBaApF (Wilt et al. 2014).

Identification

All apatites were identified by X-ray diffraction. Powder X-ray diffractograms were obtained using a PANalytical X'Pert PRO MPD (Multi-Purpose Diffractometer) Theta-Theta System with Cu-Kα radiation. A step size of 0.02° 2-theta was used with a range from 5 to 90° 2-theta. X-ray diffraction was used to confirm the identity of the compound, to detect other phases present in the samples, and to provide data for Rietveld analyses. Data for Rietveld analyses were collected with the sample in a 10 mm silicon cavity mount and scans (ca. 5-8 h) sufficient to obtain 60,000 to 100,000 counts. Further information on the Rietveld analyses is given in Wilt et al. (2014).

Structural and compositional analyses

Unit cell parameters were determined both during Rietveld analyses and by using profile-fitting of the entire XRD pattern. The indexing method was usually McMaille (Le Bail 2004), but in some cases the Treor method (Werner et al. 1985) was employed. The unit cell candidate was chosen based on its high score, symmetry, and absence of un-indexed peaks. Uncertainties in unit cell parameters were generally ±0.0007 Å, but repeated measurements on the same sample suggest a higher uncertainty of *ca*. ± 0.001 Å.

Weight percent carbon was determined by Galbraith Laboratories, Knoxville, TN using a C-, H-, N- elemental analyzer after combustion at 950°C in oxygen. The reported carbon concentrations have a relative experimental error of ±0.3 wt%. Other analyses have been reported in papers describing the syntheses and characterization of the apatites (Pasteris et al. 2014, Sternlieb et al. 2010, Weidner et al. 2014, Wilt et al. 2014, Yoder et al. 2012b, ,].

Thermogravimetric analyses were performed using TA Instruments TGA Q500. Thermograms were obtained using a balance flow of 40 mL/min of N_2, a sample flow of 60 mL/min, and the sample was heated to 1000°C at a rate of 15°C/min.

Raman spectra were obtained on four samples of each carbonated apatite to further characterize the phosphate phase and to detect contaminating phases at a lower concentration than that detected by powder X-ray diffraction. The confocal Raman system used in this study is an integrated, fiber-optically coupled microscope-spectrometer-detector from Kaiser Optical (Ann Arbor, Michigan). The HoloLab Series Research Raman

Spectrometer configured for 532-nm laser excitation simultaneously records the spectral range of 0 to 4300 Δcm^{-1}. The Andor high-resolution, thermoelectrically cooled CCD array detector provides a resolution of 2.5 cm^{-1}. Analyses of powders were made using an Olympus 80x objective with an N.A. of 0.75. Each Raman analysis represents the average of 32 acquisitions of 4 seconds each. Every sample underwent at least 6 analyses. The laser power was 10 mW at the sample surface, and the diameter of the beam was about 1 micrometer at the sample surface. The focus was optimized so as to obtain the maximum signal:noise ratio.

Determination of structural water

Each apatite was assumed to have adsorbed as well as structural water, both of which were determined by TGA. A decrease in weight of the sample from 25 to 200 °C was assumed to be due to release of adsorbed water, while structural H_2O was assumed to be released between 200 °C and 550 °C. Although structural H_2O is believed to be released even above 550 °C (Yoder et al. 2012b, Yoder et al. 2012c), decomposition to CO_2 in many carbonated apatites at approximately 600-650 °C prevents the identification of H_2O above 550 °C. The carbonate decomposition temperature depends on the nature of the cation, but for all but the lead apatites, the range of 200- 550 °C could be used to determine structural H_2O. For lead apatites, in which decomposition of carbonate occurs at 400-450 °C (Sternlieb et al. 2010), an upper limit of 350 °C was used. The amount of H_2O released in this range was then evaluated to account for the remainder of the H_2O that would have

been released up to 550 °C. This adjustment was based on the fact that an average of 45% of structural H_2O was eliminated between 350 and 550 °C in calcium apatites. The weight percent structural H_2O in each apatite was then converted to molecules per unit cell (MPUC) by first converting percent carbonate in each sample to x in the B-type substitution formula $M_{10-x}(PO_4)_{6-x}(CO_3)_x(X)_{2-x}$, producing the formula of the anhydrous portion of the apatite. The ratio of moles of H_2O to moles of anhydrous apatite was deemed equivalent to moles of H_2O per moles of unit cells, which is molecules of H_2O per unit cell (MPUC).

RESULTS AND DISCUSSION

Because all of the apatites studied were carbonated, the mode of carbonate substitution must be established. It is well known that at low temperature (< 100°C) the dominant substitution mode for calcium hydroxyl- and fluorapatites is B-type, where carbonate (CO_3^{2-}) substitutes for phosphate (PO_4^{3-}). This substitution requires charge compensation; it must be accompanied by loss or incorporation of ions (Pan and Fleet 2002). We assume that in our apatites, where sodium ions and hydrogen phosphate ions are present at low concentrations (within the limits of detection by Raman and electron microprobe analysis), charge compensation occurs by creation of cation and monovalent anion vacancies. Low proportions of A-type substitution, which involves replacement of channel X^- ions by carbonate, has been reported in some low-temperature calcium apatites. The calcium apatites prepared in our laboratory appear to have no more than ca. 5-10% A-type substitution, in accord with values reported by Elliot (2002). We assume, therefore,

that for most of the 76 apatites discussed here, the B-type substitution formula is valid. However, we have reported significant, but not dominant, A-type substitution in CSrApCl (Weidner et al. 2014), CSrApOH (Weidner et al. 2014), CPbApOH (Sternlieb et al. 2010), CPbApF (Wilt et al. 2014), and CBaApF (Wilt et al. 2014), which we will henceforth refer to as having AB-type carbonate substitution. Due to the difficulty in quantifying A-type substitution in the latter compounds (we estimate between 20 and 35% of A-type substitution based on IR peak areas), we have used the B-type substitution formula for these apatites as the best approximation to their empirical formulas.

The values of MPUC for all of the apatites studied are shown in Figure 1 as a function of the wt% carbonate in each apatite. The lack of any relationship between MPUC and wt% carbonate for the calcium apatites has been reported (Yoder et al. 2012a, Pasteris et al. 2014)) and leads to the conclusion that the average values of MPUC for calcium hydroxyl- and fluorapatites are similar at a value of somewhat less than 1.5. For strontium apatites the average value is closer to 2.0. Both the lead and barium apatites exhibit a larger spread in values than the other apatites. For lead apatites, the average value of MPUC is 1.5, whereas the average value for all of the barium apatites is about 2.5 (see Table 1 for standard deviations). Careful inspection of Figure 1 shows that for some cations, the nature of the monovalent anion also makes a difference in the number of molecules of H_2O per unit cell. For example, CBaApF appears to have a lower MPUC value than the CBaApCl and CBaApOH compounds. Although the data are limited, it also appears that the lead bromapatites have higher MPUC values than the other lead apatites.

The lack of a relationship between the concentration of carbonate and the number of H_2O molecules per unit cell of the apatite is interesting because the "clearing of the channel" that results from creation of both OH- and Ca-site vacancies in B-type substitution (Beavers and McIntyre 1946) should provide additional space in which H_2O molecules could reside. That the H_2O molecules reside in the channels is an assumption supported by Rietveld analysis and NMR analyses (Joris and Amberg 1971; Kaflak-Hachulska et al. 2003; Wilson, 2006).

The likelihood of some variation in MPUC among apatites containing different divalent cations and monovalent anions led us to examine more carefully the averages of MPUC for all synthesized apatites containing a particular cation or anion. For example the MPUC value in Table 1 for Pb is the average of the values for all CPbApF, CPbApOH, CPbApCl, and CPbApBr apatites. Likewise, the value for Cl is the average MPUC for all CCaApCl, CSrApCl, CBaApCl, and CPbApCl apatites.

The average value of MPUC (from Table 1) for each set of apatites containing a particular cation or anion is plotted against the cation or anion size in Figure 2. Although the R^2 values are only 0.83 – 0.85, there appears to be a clear dependence on the size of both the cation and anion. Because the size of the ions should be reflected in the length of the *a*- and *c*-axes of the unit cell, a subset of the 76 apatites was chosen for unit cell analysis. Table 2 shows each series, along with the number of samples in the series, for which the *a*- and *c*-axial lengths and MPUC were averaged.

These data are plotted in Figure 3, which shows a significant difference between the apatites that have nearly total B-type substitution and those that have AB-type substitution (significant A-type in addition to dominant B-type substitution): the lengths of both axes of those with nearly total B-type substitution correlate strongly with MPUC, whereas those apatites that show significant amounts of A-type substitution (AB-type) deviate considerably from the correlation lines. Indeed, the AB-type apatites have lower values of MPUC than might be expected from their cell parameters, relative to their almost exclusively B-type analogs. This differentiation of the apatites is not surprising given that the AB-type apatites contain significant amounts of carbonate ions in the channels, thereby reducing the number of water molecules that can also occupy the channel.

In Figure 3 the above information is plotted as a 3-D graph of *a*- and *c*- unit cell axial lengths on the x- and y-axes with MPUC on the z-axis. The plot makes it clear that the AB-type apatites deviate from a line that extends from CCaApOH to CBaApCl (dashed red line). The greatest deviations occur for CPbApF and CBaApF, but low values of MPUC are also evident for CSrApOH. The good correlation for B-type carbonated apatites between the number of molecules of structural H_2O present and unit cell parameters suggests that some sort of steric factor controls MPUC— more specifically, the larger the volume inside the channel the greater the number of H_2O molecules that can be accommodated. A measure of the space within the apatite channel can be obtained by calculating the empty space within the cation-defined triangles that delineate the channels. Figure 5 shows a cross-section of the *c*-axis channel in the plane of the M(2) cations in their triangular arrangement (the cation triangles are staggered by 60° moving down the **c**-axis). The distance between the

cations was obtained from Rietveld analysis of each apatite set, and the cation radii were taken to be the 6-coordinate radii of Shannon (1976). The 2-D open channel area is assumed to be the area of a circle inscribed in the triangle defined by lines connecting the centers of the channel-defining cations. The open volume of the channel space was obtained by multiplying this area by the length of the *c*-axis. Figure 6 shows the excellent correlation of MPUC with this calculated volume for each apatite set.

Other factors that could influence the stability of H_2O within the channel can be analyzed using Figure 7 as a schematic representation of an H_2O molecule and a monovalent anion X^- in the apatite channel. The anion is located at the center of the triangle defined by three cations in a plane perpendicular to the *c*-axis. Phosphate ions are shown on the outside of the channel. The major interactions between the H_2O molecule (shown in solid colors) and the other species are : a) hydrogen-bonding to the oxygen atoms of the phosphate ions lying behind the channel, though this is a fairly long-distance, and therefore a weak interaction, b) hydrogen-bonding to the X^- anion, c) charge-dipole interactions between H_2O and the cations, d) charge-dipole interaction between H_2O and the X^- anion, and e) hydrogen-bonding and dipole-dipole interactions between H_2O molecules, which may or may not be adjacent to one another. There are also other interactions such as charge-induced dipole and van der Waals that are likely less significant. The potential energies of all of the interactions are a function of the distance, r, between the H_2O molecule and the species with which it is interacting. For example, the charge-dipole interaction is the strongest interaction portrayed in this schematic, and its potential energy

varies as $1/r^2$, the magnitude of the dipole moment of H_2O, and the charge on each cation. The potential energy for each type of interaction is also determined by the orientation of the H_2O molecule, and the number of species interacting with the H_2O. For example, even though the H_2O molecule in Figure 7 is shown as directly to the left of the monovalent X^- ion along the *c*-axis and must surely interact with it through a dipole-charge interaction, it is also close to three +2 cations. The interaction between the dipole moment of the H_2O molecule and the X^- ion is unfavorable as shown, because the negative end of the dipole moment of the H_2O is directed toward the negative X^- ion. However, this orientation of the H_2O molecule is likely favored in the situation shown in Figure 7 because of the stronger overall interaction of the H_2O dipole with the three cations, which requires the dipole moment to be directed toward the center of the cation triangle (where the X^- resides).

The strength of the charge-dipole interaction of H_2O with the cations and anions in the channel should vary with the distance between the H_2O molecules and the ions, which is directly related to ion size: the larger the ion, the greater the distance from the center of the H_2O dipole to the centers of ion charges, and, therefore, the weaker the interaction. Because MPUC *increases* with ion size, or, alternatively, channel volume, the charge-dipole interaction cannot be a determining factor for MPUC.

Hydrogen-bonding between H_2O and other species may be significant, but the interaction with X^- should be strongest with OH^- and F^- (the enthalpies of hydration of

these two ions, governed partly by H-bonding, are -460 and -524 kJ/mol, respectively, with a decrease in absolute value with the larger halides). Because MPUC *increases* with halide size, H-bonding to the X^- ions is not likely a controlling factor. The same argument can be made and conclusion reached about charge-dipole interactions between H_2O and the monovalent anion.

Interactions between H_2O molecules certainly should be important to the energetics of the system shown in the schematic representation in Figure 7 (where only one H_2O molecule is shown) and dependent on the number of molecules and their proximity. Experimentally, we know that the number of H_2O molecules increases as cation and anion size (or, more accurately, the channel volume) increases. Therefore, as the number of H_2O molecules increases, presumably as a result of an increase in channel volume, the interactions between the molecules, especially H-bonding, will increase and further stabilize H_2O molecules in the channel.

It would appear, then, that the predominant structural determinant of MPUC is simply the amount of space in the channels that can be occupied by H_2O molecules. It also appears that some apatites that contain larger cations than calcium have a greater percentage of A-type substitution (Wilt, et al. 2014). The presence of channel carbonate ions clearly decreases the number of molecules of H_2O in the channel, as indicated by low values of MPUC in four sets of apatites (see Figures 3, 4 and 6). Overall, we have found no significant correlation between MPUC and concentration of carbonate in the apatite, but

this generalization is likely controlled by apatites with nearly total B-type carbonate substitution. It is likely that the additional channel space produced in the accepted B-type substitution mechanism, where cation and monovalent anion vacancies accompany carbonate substitutions for phosphates, does not lead to an increase in H_2O molecules in the channels. This hypothesis can be rationalized by assuming that, during the formation of the nascent crystallites during aqueous synthesis, H_2O molecules are incorporated into the incipient structure before carbonate. An alternative explanation is provided by the observation that apatites are slow to rehydrate after removal of water as we have previously reported (Yoder et al. 2012a). The incipient structure could be a crystalline or amorphous precursor, or both (Termine 1972; Brown and Chow 1976; LeGeros 2001; Weiner 2006; Crane et al. 2006).

In A-type carbonate substitution, carbonate ions could preempt or displace H_2O molecules in the channel. Due to the electrostatic interaction of the -2 charge on the carbonate ion with the +2 charge on the channel cations, the carbonate ion is likely to be more thermodynamically stable in the channel than is the neutral H_2O molecule. Thus, it would appear that the presence of H_2O in the channel should not prevent carbonate from entering the channel. However, there are no apatites synthesized below 100 °C, to our knowledge, that have predominant A-type substitution. (These low-temperature synthetic apatites also were synthesized aqueously.) The "reluctance" of carbonate to enter the channel (rather than substitute for phosphate), in spite of its thermodynamically greater stability in the channel may be due to the spatial difficulty of the larger carbonate ion to

enter the channels (the thermochemical radius of carbonate is 1.8 Å, whereas H_2O has an effective radius of 1.4 Å if hydrogen-bonded (Graziano, 2004)). Hence, the relatively low abundance of A-type substitution in all apatites studied to date may be either a kinetic effect, as described above, or, it may have a thermodynamic origin that depends on the relative stabilities of the hydrated ions involved in the substitution process that occurs during synthesis (Wilt et al., 2014). In first identifying the two modes of carbonate substitution in CCaApOH samples, LeGeros et al. (1969) remarked that the only way to synthesize predominantly A-type carbonated apatite was through synthesis at high temperature and with the exclusion of water.

Implications

We speculate that the volume of the channels in apatites affects the ability of H_2O molecules to occupy channel sites. In most low-temperature, aqueously precipitated $M_{10}(PO_4)_6X_2$ apatites that have been studied, carbonate prefers to substitute for phosphate rather than be incorporated into the channel sites, even though it is more thermodynamically stable in the channel relative to the sites typically occupied by phosphate (Peroos et al. 2006). For a particular species of apatite, such as $Ca_{10}(PO_4)_6(OH)_2$ or $Sr_{10}(PO_4)_6F_2$, that have nearly total B-type carbonate substitution, there is no correlation between the number of molecules of H_2O in the channels and the weight percent carbonate in the apatite. This lack of correlation would be expected when there is no competition within the channel between H_2O and carbonate. For different apatite species, that is, different sets of M and X in the formula $M_{10}(PO_4)_6X_2$, the number of H_2O

molecules in the channel depends on the volume of the channel—the greater the volume, the greater the MPUC.

In some apatites with larger ions, the ease of A-type carbonate incorporation in the channels increases, competition between H_2O and carbonate ions occurs, and some H_2O molecules are precluded or displaced to accommodate carbonate ions, which are thermodynamically more stable than H_2O in the channel. We further speculate that these scenarios are most easily rationalized by incorporation of H_2O early in the formation of nascent crystallites or another precursor phase of apatites formed in aqueous solution at temperatures below 100 °C, with carbonate entering the newly formed channels later and with some difficulty.

References

Beevers, C.A., and McIntyre, D.B. (1946) The atomic structure of fluor-apatite and its relation to that of tooth and bone material. Mineralogical Magazine, 27, 254–257.

Brown, W.E., and Chow, L.C. (1976) Chemical properties of bone mineral. Annual Review of Materials Science, 6, 213–236.

Crane, N.J., Popescu, V., Morris, M.D., Steenhuis, P., and Ignelzi, M.A. (2006) Raman spectroscopic evidence for octacalcium phosphate and other transient mineral species deposited during intramembranous mineralization. Bone, 39, 434–442.

Elliott, J.C. (2002) Calcium phosphate biominerals. In M.J. Kohn, J. Rakovan and J.M. Hughes, Eds., Phosphates -- Geochemical, Geobiological, and Materials Importance, **48**, p. 427-453. Reviews in Mineralogy and Geochemistry, Mineralogical Society of America, Chantilly, Virginia.

Flora, N.J., Hamilton, K. W., Schaeffer, R. W., and Yoder, C.H. (2004) A Comparative study of the synthesis of calcium, strontium, barium, cadmium, and lead apatites in aqueous solution, Synthesis and Reactivity in Inorganic and Metal-Organic Chemistry**,** 34, 503-521.

Graziano, G. (2004) Water: Cavity size distribution and hydrogen bonds. Chemical Physics Letters, 396, 226-231.

Hughes, J.M., Cameron, M., and Crowley, K.D. (1989) Structural variations in natural F, OH, and Cl apatites. American Mineralogist, 74, 870-876.

Hughes, J.M. and Rakovan, J. (2002) The crystal structure of apatite, $Ca_5(PO_4)_3(F,OH,Cl)$. In M.J. Kohn, J. Rakovan, and J.M. Hughes, Eds., Phosphates -- Geochemical, geobiological, and materials importance, 48, p. 1-12. Reviews in Mineralogy and

Geochemistry, Mineralogical Society of America, Chantilly, Virginia.

Joris, S.J. and Amberg, C.H. (1971) The nature of deficiency in nonstoichiometric hydroxyapatites. II. Spectroscopic studies of calcium and strontium hydroxyapatites. Journal of Physical Chemistry, 75, 3172-3178.

Kaflak-Hachulska, A., Samoson, A., and Kolodziejski, W. (2003) ^{1}H MAS and ^{1}H to ^{31}P CP/MAS NMR study of human bone mineral. Calcified Tissue International, 73, 476-486.

Le Bail, A. (2004) Monte Carlo indexing with McMaille, Powder Diffraction, 19, 249-254.

LeGeros, R.Z., Trautz, O.R., Lkein, E., and LeGeros, J.P. (1969) Two types of carbonate substitution in the apatite structure. Experimentia, 25, 5-7.

LeGeros, R.Z. (2001) Formation and transformation of calcium phosphates: Relevance to vascular calcification. Zeitschrift für Kardiologie, Suppl. 2, III116-III124.

Pan, Y., and Fleet, M.E. (2002) Composition of the apatite-group minerals: Substitution mechanisms and controlling factors. In Kohn, M.J., Rakovan, J., and Hughes, J.M., Eds. Phosphates-Geochemical, geobiological, and materials importance, 48, p. 13-49. Reviews in mineralogy and geochemistry, Mineralogical Society of America, Chantilly, Virginia.

Peroos, S., Du, Z., and de Leeuw, N. H. (2006) A computer modeling study of the uptake, structure and distribution of carbonate defects in hydroxyl-apatite. Biomaterials, 27, 2150-2161.

Pasteris, J.D., Yoder, C. H., and Wopenka, B., (2014) Molecular water in nominally unhydrated carbonated hydroxylapatite: The key to a better understanding of bone mineral, American Mineralogist, *99*, 16-27.

Pasteris, J.D., Yoder, C.H., Sternlieb, M. P., and Liu, S. (2012) Effect of carbonate incorporation on the hydroxyl content of hydroxylapatite, Mineralogical Magazine, *76*, 2741-2759.

Shannon, R.D. (1976) Revised effective ionic-radii and systematic studies of interatomic distances in halides and chalcogenides. Acta Crystallographica Section A, 32, 751-767.

Sternlieb, M.P., Pasteris, J.D., Williams, B.R., Krol, K.A., and Yoder, C.H. (2010) The structure and solubility of carbonated hydroxyl- and chloro lead apatites. Polyhedron, 29, 2364-2372.

Termine, J.D., and Lundy, D.R. (1973) Hydroxide and carbonate in rat bone mineral and its synthetic analogues. Calcified Tissue International, 13, 73–82.

Weidner, V.L., Carney, M.C., Pasteris, J.D., and Yoder, C.H. (2014) A-Type substitution in carbonated strontium fluor-, chlor-, and hydroxylapatites, Mineralogical Magazine, in revision.

Weiner, S. (2006) Transient precursor strategy in mineral formation of bone. Bone, 39, 431–433.

Werner, P.-E., Eriksson, L. and Westdahl, M. (1985) Treor, a semi-exhaustive trial-and-error powder indexing program for all symmetries. Journal of Applied Crystallography, 18, 367-370

Wilson, R.M., Dowker, S.E.P., and Elliott, J.C. (2006) Rietveld refinements and spectroscopic structural studies of a Na-free carbonate apatite made by hydrolysis of monetite. Biomaterials, 27, 4682-4692.

Wilt, Z., Fuller, C., Bachman, T., Weidner, V., Pasteris, J.D., and Yoder, C.H. (2014) Synthesis and structure of carbonated heavy metal (Ba, Pb) fluorapatites: Effect of cation size on A-type carbonate substitution, American Mineralogist, in press.

Yoder, C., Pasteris, J., Worcester, K., Schermerhorn, D., Sternlieb, M., Goldenberg, J., and Wilt, Z. (2012a) Dehydration and rehydratiom of carbonated fluor- and hydroxylapatite. Minerals, 2, 85-99.

Yoder, C. H., Pasteris, J.D., Krol, K.A., Weidner, V. L, and Schaeffer, R. W., (2012b) Synthesis, structure, and solubility of carbonated barium chlor- and hydroxylapatites. Polyhedron, 44, 143-149.

Yoder, C.H., Pasteris, J.D., Worcester, K.N., and Schermerhorn, D.V. (2012c) Structural water in carbonated hydroxylapatite and fluorapatite: confirmation by solid state ^{2}H NMR, Calcified Tissue International, 90, 60-67.

Tables

Table 1. The average number of H_2O molecules per unit cell (MPUC) for all apatites containing a particular cation or anion. Ionic radii are 6-coordinate radii given by Shannon (1976).

Series	Ion Size Å	Average MPUC	Standard Deviation	Number in series
Ca	1.00	1.50	0.02	25
Sr	1.18	2.06	0.16	15
Pb	1.19	1.65	0.71	23
Ba	1.35	2.49	0.96	13
F	1.33	1.47	0.49	33
Cl	1.81	2.22	0.88	12
Br	1.96	2.83	0.35	3
OH	1.37	1.96	0.57	28

Table 2. Apatite sets for which cell parameters and MPUC were averaged. Each set contains apatites with a range of carbonate concentrations. The apatite sets are grouped into those with nearly total B-type carbonate substitution and those (AB-type) for which

there is evidence from both IR and Rietveld analysis of significant A-type in addition to dominant B-type substitution. The inability to obtain good cell parameters for some compounds in the CPbApBr and CBaApCl series reduced the number of samples in these sets and MPUC for these series must be assigned greater uncertainties. Uncertainties in the average axial lengths are *ca*. ± 0.01 Å.

Apatite		Samples in set	Av. a-axis Å	Av. c-axis, Å	Av. MPUC
B-type	CCaApOH	3	9.36	6.93	1.67
	CCaApF	4	9.34	6.90	1.53
	PbApBr	1	10.01	7.41	3.2
	PbApOH	3	9.89	7.44	3.25
	BaApCl	1	10.27	7.67	4.0
	SrApF	4	9.72	7.29	2.24
AB-type	PbApF	6	9.84	7.39	0.93
	BaApF	3	10.16	7.73	0.84
	SrApCl	3	9.85	7.23	1.85
	SrApOH	3	9.79	7.29	1.84

Figure captions

Figure 1. The relationship between number of H_2O molecules per unit cell MPUC and wt% carbonate in carbonated apatites of calcium, strontium, barium, and lead.

Figure 2. Average MPUC for all apatites containing a given cation or anion vs. the cation or anion size. MPUC values were averaged for all compounds containing a particular cation or anion (see Table 1).

Figure 3. Average MPUC for 10 sets of apatites (data given in Table 2) plotted against the average *a*- and *c*-axial lengths for each set of apatites. Uncertainties in the average axial lengths are *ca*. ± 0.01 Å. The apatites in each set contain a range of carbonate concentrations. Solid diamonds represent those apatite sets for which B-type carbonate substitution is > 90%; hollow diamonds represent those apatite sets for which the apatites have significant, but not dominant concentrations of A-type carbonate in the channels.

Figure 4. Correlation of **a**- and **c**- unit cell axial lengths with MPUC. Uncertainties in the average axial lengths are *ca*. ± 0.01 Å. Colors indicate level of MPUC values.

Figure 5. Two-dimensional approximation of the free channel space as the area of the circle inscribed into the M(2)-defined triangle.

Figure 6. Correlation of MPUC with channel volume (area, determined as shown in Figure 5, multiplied by c-axis length). Uncertainties in the channel volumes are *ca*. ± 0.1 $Å^3$.

Figure 7. A schematic representation of possible interactions within the apatite channel. The water molecule is depicted with a red oxygen and blue hydrogen atoms and an arrow depicting the dipole moment of the molecule. The calcium ions are shown arranged in a triangle around the monovalent anion with the water molecule closer to the reader inside the channel. The phosphate ions lie outside of the channel.

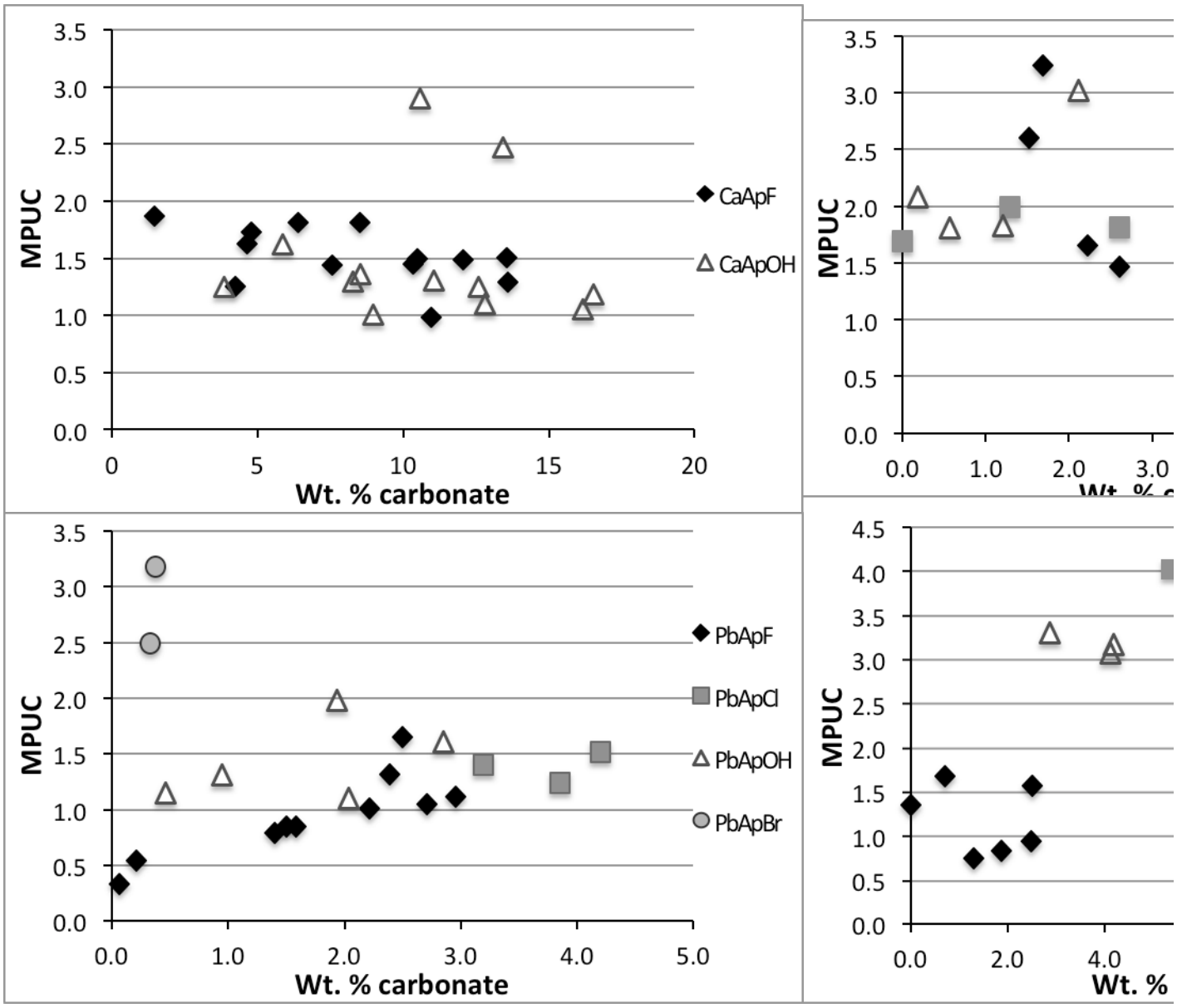
MPUC
Wt. % carbonate
CaApF
CaApOH
PbApF
PbApCl
PbApOH
PbApBr
Wt. %

Fig. 1

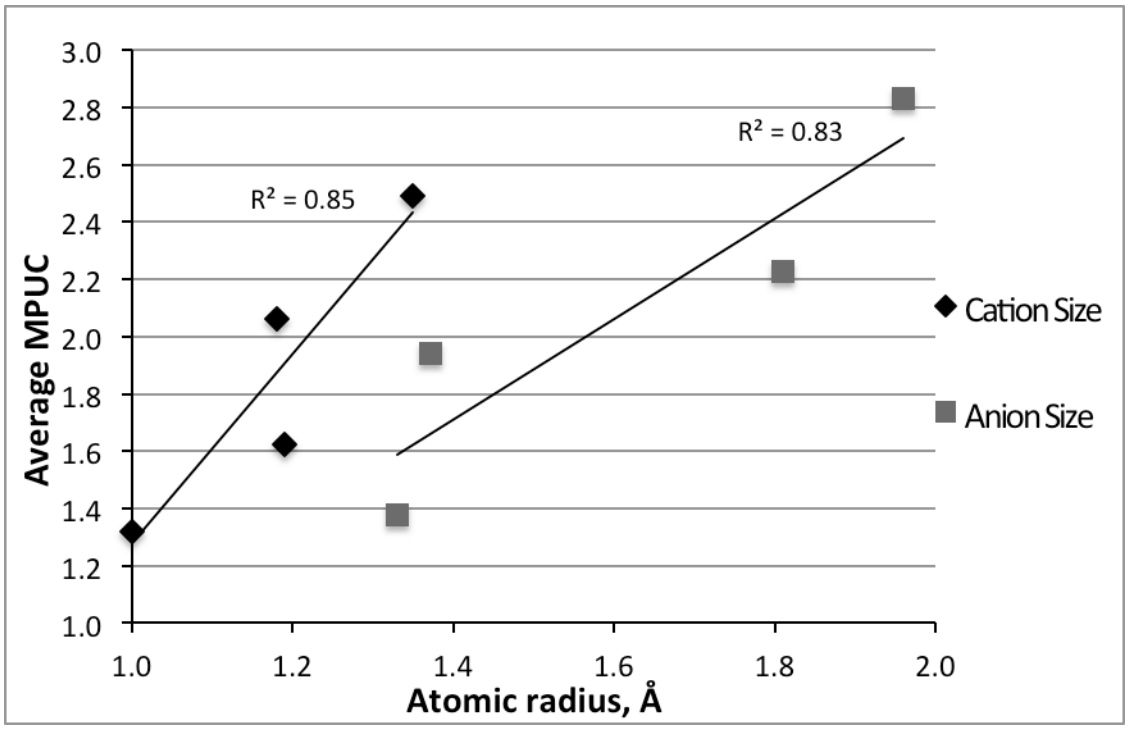
Average MPUC
Atomic radius, Å
R² = 0.85
R² = 0.83
Cation Size
Anion Size
3.0
2.8
2.6
2.4
2.2
2.0
1.8
1.6
1.4
1.2
1.0
1.0
1.2
1.4
1.6
1.8
2.0

Fig. 2

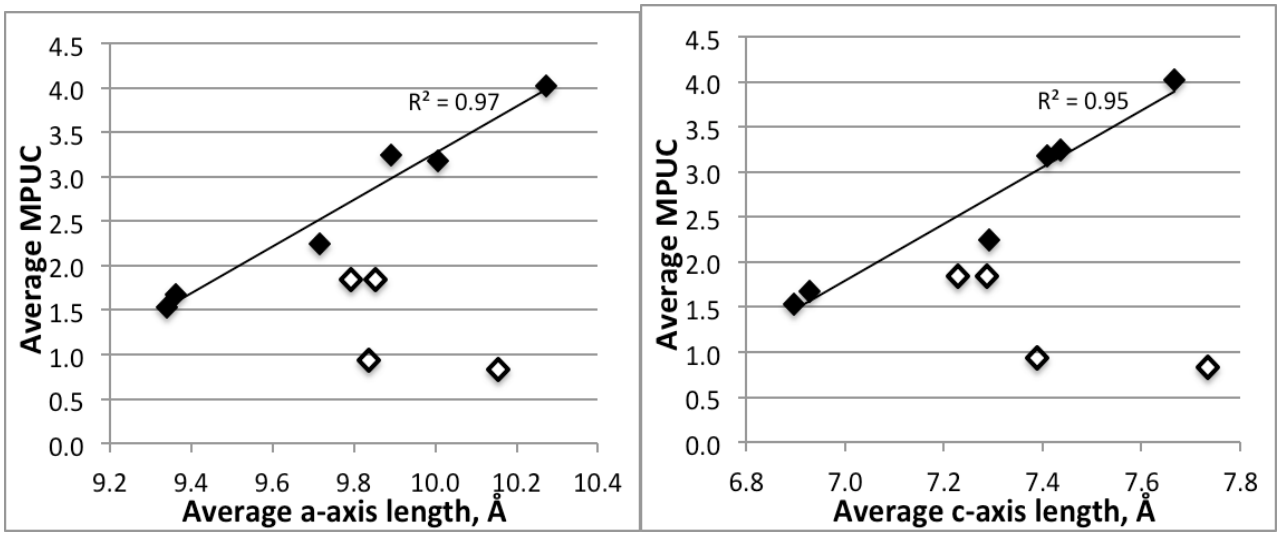
Average MPUC
Average a-axis length, Å
R² = 0.97
4.5
4.0
3.5
3.0
2.5
2.0
1.5
1.0
0.5
0.0
9.2
9.4
9.6
9.8
10.0
10.2
10.4
Average MPUC
Average c-axis length, Å
R² = 0.95
6.8
7.0
7.2
7.4
7.6
7.8

Fig. 3

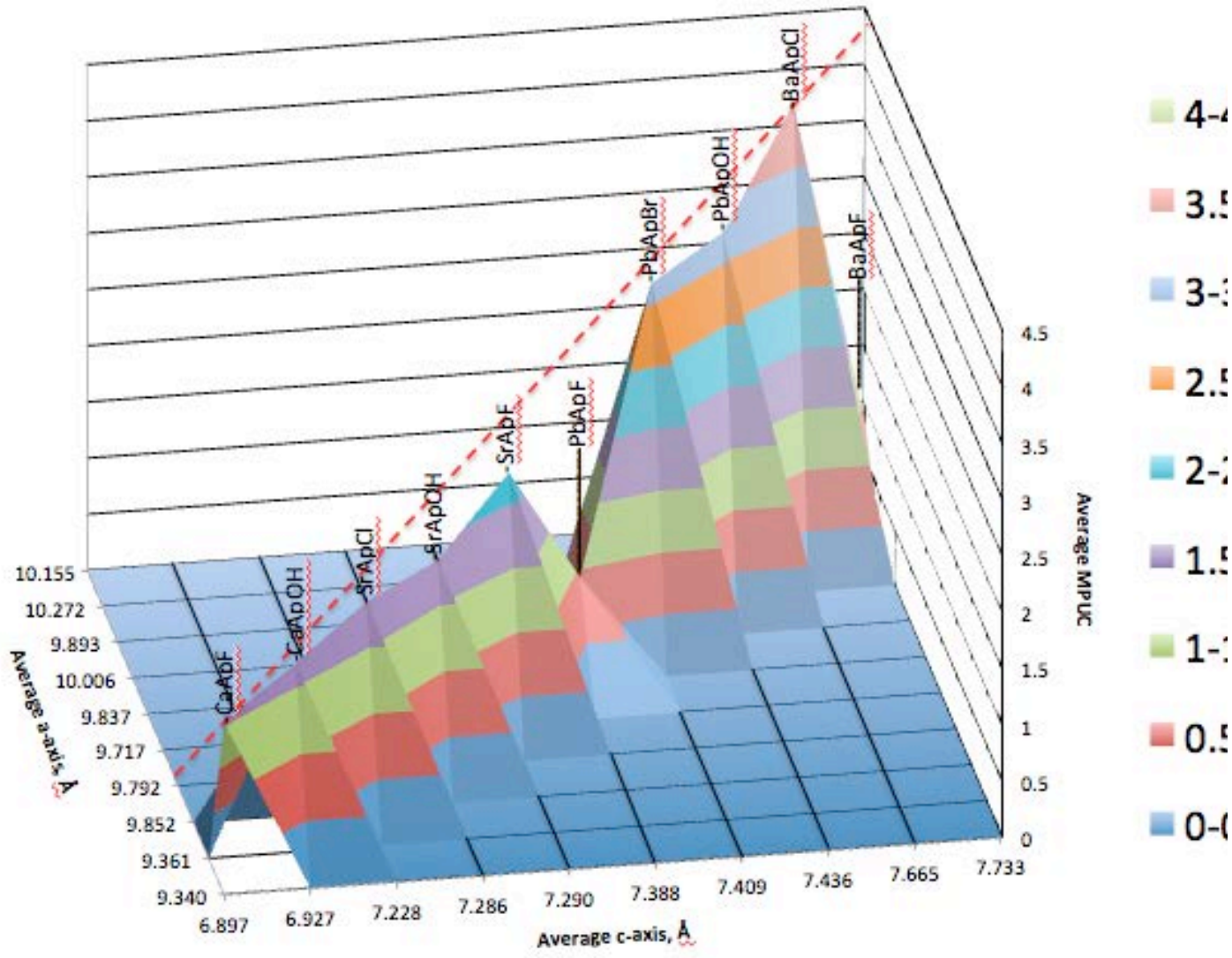
BaApCl
PbApOH
PbApBr
BaApF
SrApF
PbApF
SrApOH
SrApCl
CaApOH
CaApF
10.155
10.272
9.893
10.006
9.837
9.717
9.792
9.852
9.361
9.340
Average a-axis, Å
6.897
6.927
7.228
7.286
7.290
7.388
7.409
7.436
7.665
7.733
Average c-axis, Å
4.5
4
3.5
3
2.5
2
1.5
1
0.5
0
Average MPUC

Fig. 4

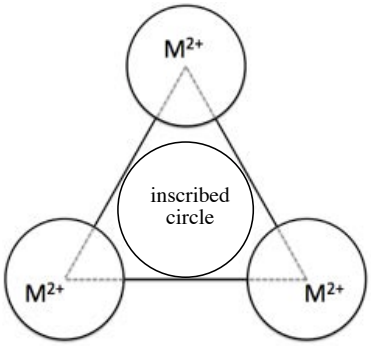
M2+
inscribed circle
M2+
M2+

Fig. 5

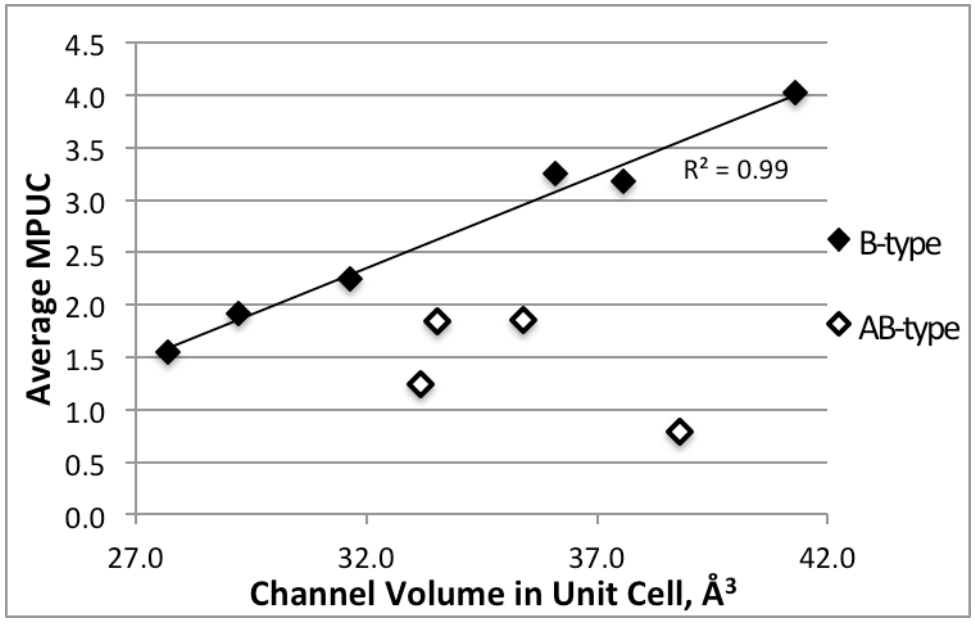
4.5
4.0
3.5
3.0
2.5
2.0
1.5
1.0
0.5
0.0
Average MPUC
R² = 0.99
B-type
AB-type
27.0
32.0
37.0
42.0
Channel Volume in Unit Cell, Å³

Fig. 6

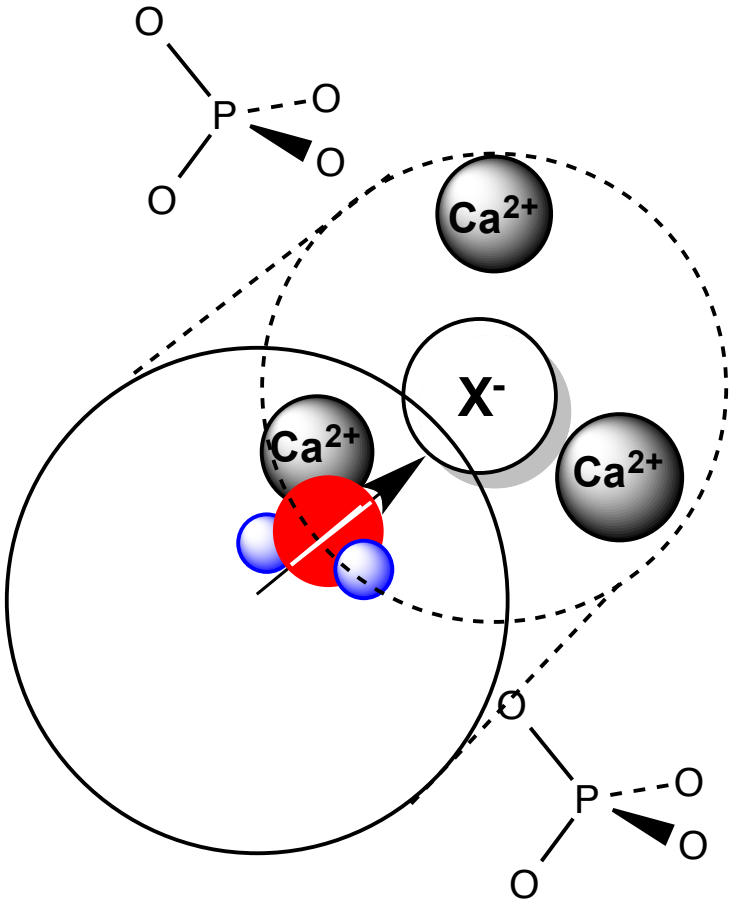

Fig. 7